Time-delay interferometry and clock-noise calibration

Massimo Tinto[*]
University of California San Diego, Center for Astrophysics and Space Sciences, 9500 Gilman Drive, La Jolla, California 92093, USA

Olaf Hartwig[†]
Max-Planck-Institut für Gravitationsphysik (Albert-Einstein-Institut), Callinstraße 38, 30167 Hannover, Germany

(Received 6 July 2018; published 21 August 2018)

The Laser Interferometer Space Antenna is a joint European Space Agency–NASA space mission to detect and study milliherz cosmic gravitational waves. The trajectories followed by its three spacecraft result in unequal- and time-varying arms, requiring use of the time-delay interferometry (TDI) postprocessing technique to cancel the laser phase noises affecting the heterodyne one-way Doppler measurements. Although the second-generation formulation of TDI cancels the laser phase noises when the array is both rotating and "flexing," second-generation TDI combinations for which the phase fluctuations of the onboard ultrastable oscillators can be calibrated out have not appeared yet in the literature. In this article, we present the solution of this problem by generalizing to the realistic LISA trajectory the ultrastable oscillators calibration algorithm derived by Tinto *et al.* for a static configuration.

DOI: 10.1103/PhysRevD.98.042003

I. INTRODUCTION

Gravitational waves (GWs) are predicted by Einstein's theory of general relativity and represent disturbances of space-time propagating at the speed of light. Because of their extremely small amplitudes and interaction cross sections, GWs carry information about regions of the Universe that would be otherwise unobtainable through the electromagnetic spectrum. Their first detection announced by the LIGO project in February 2016 [1], followed by the additional observations of four more events [2–5], marked the beginning of GW astronomy.

Contrary to ground-based laser interferometers, which are sensitive to GWs in a band from about a few tens of hertz to a few kilohertz, space-based interferometers are expected to access the frequency region from a few tenths of millihertz to about a few tens of hertz, where GW signals are expected to be larger in number and characterized by larger amplitudes. The most notable example of a space-based interferometer, which for several decades has been jointly studied in Europe and in the United States of America, is the Laser Interferometer Space Antenna (LISA) mission [6]. LISA, which is now expected to be launched in the year 2034, will detect and study cosmic gravitational waves in the $10^{-4} - 1$ Hz band by relying on coherent laser beams exchanged by three remote spacecraft along the arms of their forming giant (almost) equilateral triangle of 2.5×10^6 km arm length.

A space-based laser interferometer GW detector measures relative frequency changes experienced by coherent laser beams exchanged by three pairs of spacecraft. As the laser beams are received, they are made to interfere with the outgoing laser light. Since the received and receiving frequencies of the laser beams can be different by tens to perhaps hundreds of millihertz (consequence of the Doppler effect from the relative interspacecraft velocities and the intrinsic frequency differences of the lasers), to remove these large beat notes present in the heterodyne measurements, one relies on the use of a microwave signal generated by an onboard clock [usually referred to as the ultrastable oscillator (USO)]. The magnitude of the frequency fluctuations introduced by the USO into a heterodyne base-band one-way Doppler measurement depends linearly on the USO's noise itself and the heterodyne beat-note frequency. The USO baselined by the LISA project relies on an oven-stabilized crystal and is characterized by an Allan standard deviation of $\sigma_A \approx 10^{-13}$ for averaging times in the interval $1 - 10^4$ s, covering the frequency band of interest to space-based interferometers [6]. In the case of the LISA mission, in particular, it was estimated [7] that the magnitude of the square root of the power spectral density of the USO's relative frequency fluctuations appearing, for instance, in the unequal-arm Michelson time-delay interferometry (TDI) combination X (valid for a static-array configuration) would be about 3 orders of magnitude larger

[*]mtinto@ucsd.edu
[†]olaf.hartwig@aei.mpg.de

than that due to the residual (optical-path and proof-mass) noise sources.

A technique for removing the USO noise from a Michelson interferometer for a static-array configuration was first discussed in Ref. [8], applied in Ref. [9] to the unequal-arm Michelson X and Sagnac α TDI combinations for a static array (TDI-1), and improved and extended to all the TDI-1 combinations in Ref. [7]. This technique requires the modulation of the laser beams exchanged by the spacecraft and the further measurement of six more interspacecraft relative phases by comparing the sidebands of the received beam against sidebands of the transmitted beam. The physical reason behind the use of modulated beams for calibrating the USOs noises is to exchange the USOs phase fluctuations so they can experience the same time delays as those experienced by the laser phase noises while propagating along the three arms.[1] By performing sideband-sideband measurements [7–9], six additional one-way phase differences that allow one to calibrate out the USOs phase fluctuations from the TDI-1 combinations while preserving the gravitational wave signal in the resulting USO-calibrated TDI data are generated.

Although an alternative experimental implementation to the modulation technique, which relies on the use of an onboard optical-frequency comb [10–12] to generate the microwave frequency coherent to the frequency of the onboard laser,[2] has recently been proposed [13], in this article, we derive the TDI combinations for a rotating and "flexing" array [so-called second-generation TDI (TDI-2)] that calibrate out the microwave signal phase fluctuations due to the onboard LISA USOs. A summary of this article is presented below.

In Sec. II, we provide the mathematical expressions describing the one-way heterodyne base-band measurements performed onboard the LISA spacecraft. They reflect the planned LISA's split-interferometry design, and they were first presented in Refs. [14,15]. In these references, a data processing algorithm was also proposed to obtain TDI-2 combinations that are USO noise free. Recently, however, it has been shown (by the LISA Simulation Working Group) that the technique discussed in Refs. [14,15] does not work as expected, and we discuss the physical reasons behind its shortcoming.

After showing that the commutator of two delay operators applied to the phase noise of a LISA USO results in relative frequency fluctuations (strain) that are significantly smaller than those associated with the acceleration and optical-path noises, in Sec. III, we derive the expressions that calibrate the USO noises out of the TDI-2 unequal-arm Michelson and Sagnac interferometric combinations [16]. A summary of our results and conclusions are then presented in Sec. IV.

II. SPLIT-INTERFEROMETRY ONE-WAY HETERODYNE MEASUREMENTS

In what follows, we provide the expressions for the eight one-way heterodyne base-band measurements performed by the phase meter onboard spacecraft 1; the remaining 16 can be obtained by cyclic permutation of the spacecraft indices. As pointed out in Refs. [14,15], the base-band process performed by the phase meter amounts to measuring the *absolute value* of the difference between the received and receiving frequencies of the lasers beams made to interfere at the photodetectors. This is done through the use of a numerically controlled microwave frequency referenced to the onboard USO [7–9]. Since the operational frequency band of a LISA's photodetector ranges from about 5 (below this frequency, the relative intensity noise becomes excessive) and 25 MHz (above this frequency, the digitization noise becomes unacceptably large) and because of the additional $\approx \pm 10$ MHz Doppler shift between the frequencies of two interspacecraft lasers, it is necessary to transmit and receive laser beams of which the frequency differences fall within the photodetectors' operational bandwidth. By implementing high-accuracy frequency stabilization methods [17,18] and/or frequency locking schemes [6], and by relying on a predefined frequency allocation plan, one can then have the frequency beat notes fall within the operational bandwidths of the photodetectors, infer the correct sign of the beat-note frequencies, and further process the base-band data [14,19]. The expressions of the base-band measurements performed by the phase meter were derived in Refs. [14,15] in the context of the LISA split-interferometry architecture, and we refer the reader to those publications for more details. Here, we adopt those expressions and modify them by accounting for the correct sign of the frequency differences as given by the frequency allocation plan. This amounts to multiplying both sides of the equations given in Refs. [14,15] by the signs of the frequency differences as specified by the frequencies allocation plan. An example application of what we just described can be found in Ref. [14] (see p. 124 there), in which the signs of the various frequency differences, denoted there by the symbols θ_{ij}, are discussed. These are functions of the laser phase lock offset frequencies and interspacecraft Doppler shifts. They are equal to either $+1$ or -1, depending on whether the frequency of the received beam, ν_i, is larger or smaller than the frequency ν_j of the receiving beam, respectively.

We adopt the description of the LISA array given in Ref. [16], in which the beam arriving at spacecraft i has subscript i and is primed or unprimed depending on

[1]Although dispersive effects in the measurement chain could add additional delays, they are expected to be either negligible or characterizable. For this reason, they have been disregarded in our discussion.

[2]The optical frequency-comb technique exactly cancels the microwave signal phase fluctuations as it relies on modified TDI-2 combinations and does not require the use of modulated beams.

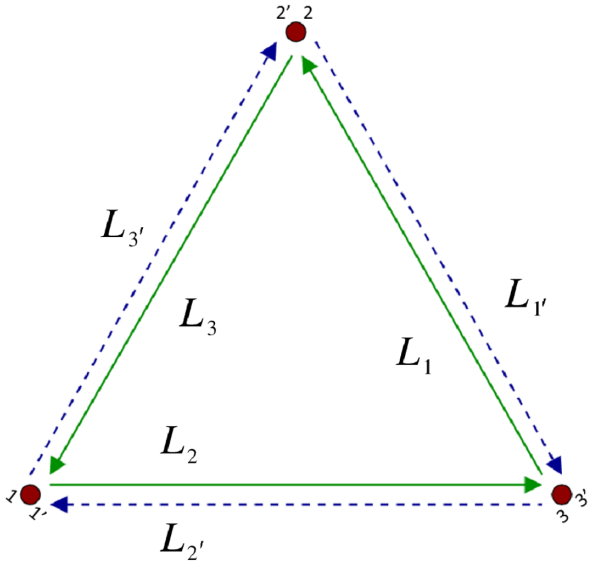

FIG. 1. Schematic LISA configuration. The spacecraft are labeled 1, 2, and 3, with their optical benches labeled with primed or unprimed indices depending on whether the received laser beam is propagating clockwise or counterclockwise as seen from above the plane of the picture. The optical paths are denoted by L_i and $L_{i'}$, where the index i corresponds to the opposite spacecraft.

whether the beam is traveling clockwise or counterclockwise, respectively, around the LISA triangle as seen from above the plane of the constellation described in Fig. 1. We also adopt the usual notation for delayed data streams, which is convenient for algebraic manipulations [16]. We define the six time-delay operators $\mathcal{D}_i$, $\mathcal{D}_{i'}$, $i = 1, 2, 3$, $i' = 1', 2', 3'$, where for any data stream $x(t)$

$$\mathcal{D}_{j'}\mathcal{D}_i x(t) = x(t - L_i(t - L_{j'}) - L_{j'}), \tag{1}$$

where $(L_{j'}, L_i)$, $j' = 1', 2', 3'$, $i = 1, 2, 3$, are the light travel times along the three arms of the LISA triangle along the clockwise and counterclockwise directions, respectively.[3] It is important to note that, although $[\mathcal{D}_{j'}, \mathcal{D}_i]x(t) \neq 0$ in general, the commutator of two delay operators can be neglected if the resulting magnitude of a random process it is applied to is significantly smaller than the magnitude of the secondary (acceleration and optical-path) noises affecting the LISA measurements.

The eight heterodyne base-band measurements performed by the phase meter onboard spacecraft 1 are presented in two groups, each including four data sets from the specific optical bench where they are collected. The group of measurements from optical bench $1'$ is represented by the mathematical expressions (see Fig. 2)

$$s^{\mathrm{c}}_{1'} = [H_{1'} + \mathcal{D}_{2'}p_3 - p_{1'} - 2\pi\nu_3(\mathbf{n}_{2'}\cdot\mathcal{D}_{2'}\boldsymbol{\Delta}_3 + \mathbf{n}_2\cdot\boldsymbol{\Delta}_{1'}) + N^{\mathrm{obt}}_{1'}] - a_{1'}q_1 + N^{\mathrm{s}}_{1'}, \tag{2}$$

$$s^{\mathrm{sb}}_{1'} = [H_{1'} + \mathcal{D}_{2'}p_3 - p_{1'} + m_3\mathcal{D}_{2'}q_3 - m_{1'}q_1 - 2\pi\nu_3(\mathbf{n}_{2'}\cdot\mathcal{D}_{2'}\boldsymbol{\Delta}_3 + \mathbf{n}_2\cdot\boldsymbol{\Delta}_{1'}) + N^{\mathrm{obt.sb}}_{1'}] - c_{1'}q_1 + N^{\mathrm{sb}}_{1'}, \tag{3}$$

$$\epsilon_{1'} = [p_1 - p_{1'} + 4\pi\nu_1(\mathbf{n}_2\cdot\boldsymbol{\delta}_{1'} - \mathbf{n}_2\cdot\boldsymbol{\Delta}_{1'}) + \mu_1] - b_{1'}q_1 + N^{\epsilon}_{1'}, \tag{4}$$

$$\tau_{1'} = [p_1 - p_{1'} + \mu_1] - b_{1'}q_1 + N^{\tau}_{1'}, \tag{5}$$

while those from optical bench 1 are equal to

$$s^{\mathrm{c}}_1 = [H_1 + \mathcal{D}_3 p_{2'} - p_1 - 2\pi\nu_{2'}(\mathbf{n}_3\cdot\mathcal{D}_3\boldsymbol{\Delta}_{2'} + \mathbf{n}_{3'}\cdot\boldsymbol{\Delta}_1) + N^{\mathrm{obt}}_1] - a_1 q_1 + N^{\mathrm{s}}_1, \tag{6}$$

$$s^{\mathrm{sb}}_1 = [H_1 + \mathcal{D}_3 p_{2'} - p_1 + m_{2'}\mathcal{D}_3 q_2 - m_1 q_1 - 2\pi\nu_{2'}(\mathbf{n}_3\cdot\mathcal{D}_3\boldsymbol{\Delta}_{2'} + \mathbf{n}_{3'}\cdot\boldsymbol{\Delta}_1) + N^{\mathrm{obt.sb}}_1] - c_1 q_1 + N^{\mathrm{sb}}_1, \tag{7}$$

$$\epsilon_1 = [p_{1'} - p_1 + 4\pi\nu_{1'}(\mathbf{n}_{3'}\cdot\boldsymbol{\delta}_1 - \mathbf{n}_{3'}\cdot\boldsymbol{\Delta}_1) + \mu_{1'}] - b_1 q_1 + N^{\epsilon}_1, \tag{8}$$

$$\tau_1 = [p_{1'} - p_1 + \mu_{1'}] - b_1 q_1 + N^{\tau}_1. \tag{9}$$

The observables s^{c}, s^{sb}, ϵ, and τ are the interspacecraft carrier-to-carrier and sideband-to-sideband one-way heterodyne base-band measurements, the proof mass-to-optical bench, and the bench-to-bench metrology measurements, respectively; the a, b, and c are the fractional frequency beat-note coefficients, i.e., the coefficients determined by the phase meter [15] that multiply the USO-referenced pilot-tone frequency so as to match the beat-note frequencies. The expressions of these coefficients are obtained from the corresponding ones given in Ref. [15] by multiplying them by the appropriate signs of the frequency differences defined by the frequency allocation plan (these are the "sign functions" θs in Ref. [15]). After performing such operation, it is easy to show that they become equal to

[3]The speed of light c is assumed to be unity in this article.

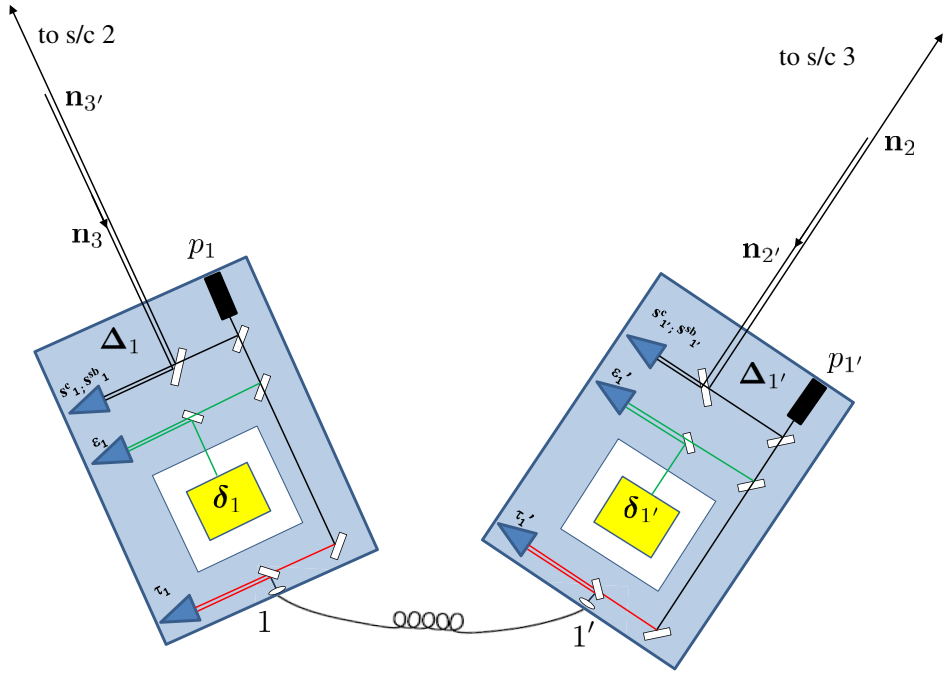

FIG. 2. Simplified schematic diagram of the proof mass and optical bench assemblies for LISA spacecraft 1. The left bench reads out a phase signal s_1^{c} from optical bench $2'$ onboard spacecraft 2. The phase difference is measured by using the laser, the photodetector on the left optical bench, and the phase meter (not shown), where the base-band and digitization of the one-way measurements is performed. The motion of the optical bench relative to the proof mass is measured through internal metrology and results in the time series ϵ_1. The relative phase fluctuations between the laser on the optical bench 1 and the laser on the optical bench $1'$ are instead captured by the measurements τ_1 and $\tau_{1'}$, respectively. Finally, the sideband-sideband phase differences, s_1^{sb} and $s_{1'}^{\mathrm{sb}}$, capture the phase fluctuations of the USOs onboard spacecraft 2 and 3, respectively, relative to those of the USO onboard spacecraft 1. These are the "essential ingredients" of the USO calibration algorithm.

$$a_{1'} = \frac{\nu_3(1-\dot{L}_{2'}) - \nu_{1'}}{f_1}, \tag{10}$$

$$a_1 = \frac{\nu_{2'}(1-\dot{L}_3) - \nu_1}{f_1} \tag{11}$$

$$b_{1'} = \frac{\nu_1 - \nu_{1'}}{f_1}, \qquad b_1 = \frac{\nu_{1'} - \nu_1}{f_1} = -b_{1'} \tag{12}$$

$$c_{1'} = \frac{(\nu_3 + m_3 f_3)(1-\dot{L}_{2'}) - (\nu_{1'} + m_{1'} f_1)}{f_1}, \tag{13}$$

$$c_1 = \frac{(\nu_{2'} + m_{2'} f_2)(1-\dot{L}_3) - (\nu_1 + m_1 f_1)}{f_1} \tag{14}$$

In Eqs. (2)–(9), the H terms are the contributions to the measured phase fluctuations due to a possibly present transverse-traceless gravitational wave signal; the p and ν terms represent the lasers' phase noises and frequencies, respectively; the q terms are the phase noises due to the three USOs; the N terms are shot-noise phase fluctuations at the photodetectors; L terms and $\dot{L}$ terms are the interspacecraft relative optical paths and their time derivatives, respectively; the f terms are the USOs' pilot-tones frequencies, while the m terms are integer numbers defining the modulation frequencies [15]; the $\mathbf{n}$ terms are unit vectors along the directions of propagation of the laser beams; the $\boldsymbol{\Delta}$ terms and $\boldsymbol{\delta}$ terms are vector random processes associated with the mechanical vibrations of the optical benches and proof masses with respect to the local inertial reference frame, respectively; the μ terms are phase fluctuations due to the optical fibers linking the two optical benches, and they have been assumed to be independent of the direction of propagation of the optical beams within them (see Ref. [15] for a clear discussion about this point); finally, the $\mathcal{D}_i$ and $\mathcal{D}_{j'}$ are delay operators [16].

Since the LISA array is both rotating and flexing, two delay operators do not commute in general [16]. For instance, with a laser noise equal to 30 Hz/$\sqrt{\mathrm{Hz}}$ in the millihertz band [16], the commutator of two delay operators applied to it results in residual fluctuations that are about an order of magnitude larger than those identified by the secondary noises. This is, in fact, the reason why the formulation of TDI for a static array is unable to suppress such a laser noise below the level identified by the secondary noises.

In the case of a LISA's USO, however, its relative frequency fluctuations at optical frequency are significantly

smaller than those of a laser. This means that the commutator of two delay operators applied to it results in relative frequency fluctuations significantly smaller than those due to the secondary noises. To be more quantitative, let us estimate the magnitude of the commutator of two delay operators applied to the phase fluctuations, $q(t)$, of a LISA USO. This is given by the following expression [16]:

$$[\mathcal{D}_i, \mathcal{D}_j]q(t) = q(t - L_i(t) - L_j(t - L_i)) - q(t - L_j(t) - L_i(t - L_j)) \simeq [L_i\dot{L}_j - L_j\dot{L}_i]\dot{q}. \quad (15)$$

The right-hand side of Eq. (15) implies the order-of-magnitude estimate of the corresponding Fourier components of the relative frequency fluctuations (strain) amplitude, $\frac{\widetilde{|\Delta C_q(f)|}}{\nu_0}$, in a TDI combination

$$\frac{\widetilde{|\Delta C_q(f)|}}{\nu_0} \equiv (4\pi L\dot{L})\left(\frac{af_q}{\nu_0}\right)\left(\frac{|\tilde{\dot{q}}(f)|}{2\pi f_q}\right)f, \quad (16)$$

where the $\tilde{}$ symbol means "Fourier transform" and f is the Fourier frequency. By assuming a LISA USO characterized by a one-sided power spectral density of relative frequency fluctuations equal to $S_y(f) = 6.7 \times 10^{-27}\ f^{-1}\ \mathrm{Hz}^{-1}$,[4] a beat-note frequency of $af_q = 25$ MHz, a laser frequency of $\nu_0 = 3 \times 10^{14}$ Hz, a LISA arm length (in seconds) of $L = 8.3$ sec. and an interspacecraft characteristic relative velocity of $\dot{L} \simeq 3 \times 10^{-8}$, we find the right-hand side of Eq. (16) to be equal to $2.3 \times 10^{-26}\ \mathrm{Hz}^{-1/2}$ at $f = 1$ Hz and smaller than this value at lower frequencies. Since this is more than 5 orders of magnitude smaller than the minimum of the strain sensitivity identified by the secondary noises in the TDI-1 combinations [7], we can regard the commutator of two delay operators to be negligibly small when applied to a LISA USO phase noise.

Before deriving the USO noise calibrating expressions, it is necessary to first remove the optical bench noises from the interspacecraft one-way measurements s^c [15]. This is done by using the differences $\epsilon - \tau$ from each optical bench as they contain the displacement of the optical bench relative to the proof mass. Second, the laser phase fluctuations with primed indices, $p_{i'}$, can be expressed in terms of those with unprimed indices, p_i, by taking suitable linear combinations of the s^c_i, τ_i, τ_j. This final operation results in the so-called η combinations, which depend only on the three unprimed laser phase fluctuations, p_i [16], and are not affected by the optical-bench noise. Their expressions are equal to [15]

$$\eta_{1'} = \xi_{1'} + z_1, \quad (17)$$

$$\eta_1 = \xi_1 - \mathcal{D}_3 z_2, \quad (18)$$

where

$$\xi_{1'} \equiv s^c_{1'} - \frac{\nu_3}{\nu_1}\frac{(\epsilon_{1'} - \tau_{1'})}{2} - \frac{\nu_3}{\nu_{3'}}\mathcal{D}_{2'}\frac{(\epsilon_3 - \tau_3)}{2}, \quad (19)$$

$$\xi_1 \equiv s^c_1 - \frac{\nu_{2'}}{\nu_{1'}}\frac{(\epsilon_1 - \tau_1)}{2} - \frac{\nu_{2'}}{\nu_2}\mathcal{D}_3\frac{(\epsilon_{2'} - \tau_{2'})}{2}, \quad (20)$$

$$z_1 \equiv \frac{\tau_1 - \tau_{1'}}{2}. \quad (21)$$

As mentioned in the Introduction, recent LISA Simulation Working Group activities have shown that the current algorithm [15] to calibrate the USO noises out of the TDI-2 combinations is not performing as expected. To understand why, let us consider the one-way data measurements described by Eqs. (2)–(9). Onboard each spacecraft, there are two sets of them, one set per optical bench, with a total of 24 data measurements after including those for the split-interferometry configuration and the sideband-sideband one-way interspacecraft Doppler data. From a simple counting argument, we conclude that the number of observables is larger than the number of noises to be canceled. There are six lasers, three USOs, six optical-bench noises,[5] and six fiber-optics noises (as this may depend on the direction of the light propagation within the fiber) for a total of 21 random processes to be canceled by properly combining the 24 data set. To solve this well-posed mathematical problem, the choice was made in Ref. [15] to regard one of the USO noises to be equal to zero. This choice was based on the assumption that the USO noises enter in the heterodyne base-band measurements as simple differences and that therefore one of them could be set to zero. Unfortunately, most of the measurements do not depend on the differences of the USO noises [see Eqs. (2)–(9)]. Those that do, such as the sideband-sideband measurements, depend on differences of USO noises measured at different times. This means that, even if all USO would "glitch" equally, their differences would not cancel because of the light time delays.

As will be shown below, there exist TDI-2 combinations that cancel the laser phase fluctuations and from which it is in fact possible to calibrate out the USO noises to a sufficiently high level of precision. This is done by properly time shifting and linearly combining the η observables and the one-way carrier-to-carrier and sideband-to-sideband measurements.

[4]This one-sided power spectral density corresponds to an Allan standard deviation equal to about 10^{-13} from 1 to 10^4 sec integration times [20].

[5]Although each optical bench noise is a three-dimensional random process, only its projection along one sensitive direction is of relevance.

To minimize the length of the equations we will rely on, we will use expressions for the η observables that display only the contributions from the laser and USO noises. Under this assumption, they assume the forms

$$\eta_{1'} = \mathcal{D}_{2'} p_3 - p_1 + [-a_{1'} + b_{1'}] q_1, \tag{22}$$

$$\eta_1 = \mathcal{D}_3 p_2 - p_1 - a_1 q_1 + b_2 \mathcal{D}_3 q_2, \tag{23}$$

where the other four η observables are obtained from the above expressions by permutation of the spacecraft indices.

III. CLOCK-NOISE CALIBRATION FROM THE TDI-2 COMBINATIONS

We describe the procedure for calibrating the USO noises out of the TDI-2 combinations by deriving the expressions for the unequal-arm Michelson interferometric combination X_1 and the Sagnac combination α_1. The procedures described in this article can easily be extended to other TDI-2 combinations, and for this reason, we do not include them here.

A. X_1 combination

In terms of the η observables, the TDI-2 unequal-arm Michelson combination, X_1^{q}, is given by the expression [16]

$$\begin{aligned} X_1^{\mathrm{q}} = {} & [\mathcal{D}_3\mathcal{D}_{3'}\mathcal{D}_{2'}\mathcal{D}_2 - I][(\eta_{1'} + \mathcal{D}_{2'}\eta_3) + \mathcal{D}_{2'}\mathcal{D}_2(\eta_1 + \mathcal{D}_3\eta_{2'})] \\ & - [\mathcal{D}_{2'}\mathcal{D}_2\mathcal{D}_3\mathcal{D}_{3'} - I][(\eta_1 + \mathcal{D}_3\eta_{2'}) + \mathcal{D}_3\mathcal{D}_{3'}(\eta_{1'} + \mathcal{D}_{2'}\eta_3)], \end{aligned} \tag{24}$$

where the label $^{\mathrm{q}}$ emphasizes the USO-noise dependence. After substituting Eqs. (22) and (23) in Eq. (24), we have

$$\begin{aligned} X_1^{\mathrm{q}} = {} & [\mathcal{D}_3\mathcal{D}_{3'}\mathcal{D}_{2'}\mathcal{D}_2 - I][b_1(\mathcal{D}_{2'}\mathcal{D}_2 - I)q_1 - a_1\mathcal{D}_{2'}\mathcal{D}_2 q_1 - a_{1'}q_1 - a_{2'}\mathcal{D}_{2'}\mathcal{D}_2\mathcal{D}_3 q_2 - a_3\mathcal{D}_{2'}q_3] \\ & - [\mathcal{D}_{2'}\mathcal{D}_2\mathcal{D}_3\mathcal{D}_{3'} - I][b_1\mathcal{D}_3\mathcal{D}_{3'}(\mathcal{D}_{2'}\mathcal{D}_2 - I)q_1 - a_{1'}\mathcal{D}_3\mathcal{D}_{3'}q_1 - a_1 q_1 - a_{2'}\mathcal{D}_3 q_2 \\ & - a_3\mathcal{D}_3\mathcal{D}_{3'}\mathcal{D}_{2'}q_3]. \end{aligned} \tag{25}$$

Since the commutator of two delay operators applied to a LISA USO noise is negligibly small, we can rewrite the above equation in the form

$$\begin{aligned} X_1^{\mathrm{q}} \simeq {} & [\mathcal{D}_3\mathcal{D}_{3'}\mathcal{D}_{2'}\mathcal{D}_2 - I][b_{1'}(I - \mathcal{D}_3\mathcal{D}_{3'})(I - \mathcal{D}_{2'}\mathcal{D}_2)q_1 + a_1(I - \mathcal{D}_{2'}\mathcal{D}_2)q_1 \\ & - a_{1'}(I - \mathcal{D}_3\mathcal{D}_{3'})q_1 + a_{2'}\mathcal{D}_3(I - \mathcal{D}_{2'}\mathcal{D}_2)q_2 - a_3\mathcal{D}_{2'}(I - \mathcal{D}_3\mathcal{D}_{3'})q_3], \end{aligned} \tag{26}$$

where we have factored out the delay operator $[\mathcal{D}_3\mathcal{D}_{3'}\mathcal{D}_{2'}\mathcal{D}_2 - I]$.

It is important to note that the q terms in the square bracket in Eq. (26) can easily be related to those in Eq. (9) of Ref. [7], which are for the TDI-1 combination X of a static LISA. This means that the expressions calibrating the USO noises out of the TDI-2 combination X_1 can be derived by using the approach of Ref. [7] for the static-array unequal-arm Michelson combination X.

Following Tinto *et al.* [7], let us introduce the following linear combinations of the carrier-to-carrier and sideband-to-sideband one-way heterodyne base-band measurements:

$$r_{1'} \equiv \frac{s^{\mathrm{c}}_{1'} - s^{\mathrm{sb}}_{1'}}{m_3 f_3}, \tag{27}$$

$$r_1 \equiv \frac{s^{\mathrm{c}}_1 - s^{\mathrm{sb}}_1}{m_{2'} f_2}. \tag{28}$$

Note that the above observables differ from those given in Ref. [7] by the presence of the modulation frequency integers $m_{2'}$ and m_3. After substituting in Eqs. (27) and (28) the expressions for the one-way heterodyne base-band measurements, s^{c}, s^{sb} [Eqs. (2), (3), (6), and (7)] after some algebra, it is possible to obtain the following expressions for $r_{1'}$ and r_1:

$$r_{1'} = \frac{(1 - \dot{L}_{2'})}{f_1} q_1 - \frac{\mathcal{D}_{2'} q_3}{f_3}, \tag{29}$$

$$r_1 = \frac{(1 - \dot{L}_3)}{f_1} q_1 - \frac{\mathcal{D}_3 q_2}{f_2}. \tag{30}$$

By neglecting terms proportional to $\dot{L}$, Eq. (30) can be rewritten to sufficient precision in the form

$$r_{1'} = \frac{q_1}{f_1} - \frac{\mathcal{D}_{2'} q_3}{f_3}, \tag{31}$$

$$r_1 = \frac{q_1}{f_1} - \frac{\mathcal{D}_3 q_2}{f_2}, \tag{32}$$

with the remaining expressions obtained by cyclic permutations of the spacecraft indices. Note that the dependence

on the m integers has dropped out from the r combinations [Eqs. (31) and (32)], which are essentially equal to the corresponding ones in Ref. [7] after modifying them to account for the inequality of the delays experienced by laser beams propagating along opposite directions (Sagnac effect).

Since there are only three USO noises q_i, there exist relationships relating the six calibration data $(r_i, r_{i'})$, $i = 1, 2, 3$, $i' = 1', 2', 3'$. Because the mathematical structure of the r observables [Eqs. (31) and (32)] is equal to that of the one-way measurements in which the random processes q_i/f_i play the same role as the laser phase noises, we infer that such relationships belong to the TDI space.

By using Eqs. (31) and (32) and following Ref. [7], it is easy to derive the following identities:

$$[I - \mathcal{D}_{2'}\mathcal{D}_2]q_1 = f_1(r_{1'} + \mathcal{D}_{2'}r_3), \tag{33}$$

$$[I - \mathcal{D}_3\mathcal{D}_{3'}]q_1 = f_1(r_1 + \mathcal{D}_3 r_{2'}), \tag{34}$$

$$\mathcal{D}_3[I - \mathcal{D}_{2'}\mathcal{D}_2]q_2 = f_2[r_{1'} - (I - \mathcal{D}_{2'}\mathcal{D}_2)r_1 + \mathcal{D}_{2'}r_3], \tag{35}$$

$$\mathcal{D}_{2'}[I - \mathcal{D}_3\mathcal{D}_{3'}]q_3 = f_3[r_1 - (I - \mathcal{D}_3\mathcal{D}_{3'})r_{1'} + \mathcal{D}_3 r_{2'}]. \tag{36}$$

By first applying the delay operator $[\mathcal{D}_3\mathcal{D}_{3'}\mathcal{D}_{2'}\mathcal{D}_2 - I]$ to Eqs. (33)–(36) and substituting the resulting expressions into Eq. (26), we finally find the following USO-corrected X_1 combination:

$$\begin{aligned} X_1 \equiv X_1^{\mathrm{q}} - [\mathcal{D}_3\mathcal{D}_{3'}\mathcal{D}_{2'}\mathcal{D}_2 - I]\Big[& b_{1'}\frac{f_1}{2}[(I - \mathcal{D}_3\mathcal{D}_{3'})(r_{1'} + \mathcal{D}_{2'}r_3) + (I - \mathcal{D}_{2'}\mathcal{D}_2)(r_1 + \mathcal{D}_3 r_{2'})] \\ & + a_1 f_1[r_{1'} + \mathcal{D}_{2'}r_3] - a_{1'}f_1[r_1 + \mathcal{D}_3 r_{2'}] + a_{2'}f_2[r_{1'} - (I - \mathcal{D}_{2'}\mathcal{D}_2)r_1 + \mathcal{D}_{2'}r_3] \\ & - a_3 f_3[r_1 - (I - \mathcal{D}_3\mathcal{D}_{3'})r_{1'} + \mathcal{D}_3 r_{2'}]\Big]. \end{aligned} \tag{37}$$

Since the unequal-arm Michelson interferometric response X_1 is antisymmetric with respect to permutations of the indices (2,3'), (3,2'), and (1,1'), the corresponding combinations used for calibrating out the USO noise from X_1^{q} have been antisymmetrized by relying on Eqs. (33)–(36) and taking advantage of the "commutativity" of two delay operators applied to a LISA USO noise. The other two unequal-arm Michelson responses, X_2 and X_3, follow from Eq. (37) after performing a cyclic permutation of the spacecraft indices.

To demonstrate the efficacy of our proposed USO noise calibration procedure for the second-generation TDI combinations, in Fig. 3, we plot the square root of the power spectral densities of the relative frequency fluctuations (strain) associated with the noise sources entering the X_1 combination. These include the acceleration and optical-path noises (red line), the USO noise before it is calibrated out of X_1 (blue line), and the residual USO noise after applying the calibration procedure described in this article (green line). We chose beat-note magnitudes and signs so as to result in the worst possible USO noise spectra (blue and green lines) in the X_1 TDI combination. Note the residual USO noise is several orders of magnitude smaller than the acceleration and optical-path noises over the entire frequency band accessible by LISA.

B. α_1 combination

In terms of the η observables, the TDI-2 Sagnac combination, α_1^{q}, is given by the following expression [16]:

$$\alpha_1^{\mathrm{q}} = [\mathcal{D}_3\mathcal{D}_1\mathcal{D}_2 - I][\eta_{1'} + \mathcal{D}_{2'}\eta_{3'} + \mathcal{D}_{2'}\mathcal{D}_{1'}\eta_{2'}] - [\mathcal{D}_{2'}\mathcal{D}_{1'}\mathcal{D}_{3'} - I][\eta_1 + \mathcal{D}_3\eta_2 + \mathcal{D}_3\mathcal{D}_1\eta_3]. \tag{38}$$

After substituting Eqs. (22) and (23) in Eq. (38), we have

$$\begin{aligned} \alpha_1^{\mathrm{q}} = {} & [\mathcal{D}_3\mathcal{D}_1\mathcal{D}_2 - I][(b_{1'} - a_{1'})q_1 + \mathcal{D}_{2'}\mathcal{D}_{1'}(b_{2'} - a_{2'})q_2 + \mathcal{D}_{2'}(b_{3'} - a_{3'})q_3] \\ & - [\mathcal{D}_{2'}\mathcal{D}_{1'}\mathcal{D}_{3'} - I][(-a_1 + b_1\mathcal{D}_3\mathcal{D}_1\mathcal{D}_2)q_1 + (-a_2 + b_2)\mathcal{D}_3 q_2 \\ & + (-a_3 + b_3)\mathcal{D}_3\mathcal{D}_1 q_3]. \end{aligned} \tag{39}$$

Following a reasoning similar to the one made earlier to evaluate the commutator of two delay operators applied to a USO noise, it is easy to show that also $(\mathcal{D}_{3'}\mathcal{D}_{2'}\mathcal{D}_{1'} - \mathcal{D}_3\mathcal{D}_2\mathcal{D}_1)q \simeq 0$, where the $\simeq 0$ means it results in relative frequency fluctuations (strain) significantly smaller than those identified by the acceleration and optical-path noises. Equation (39) can therefore be rewritten in the form

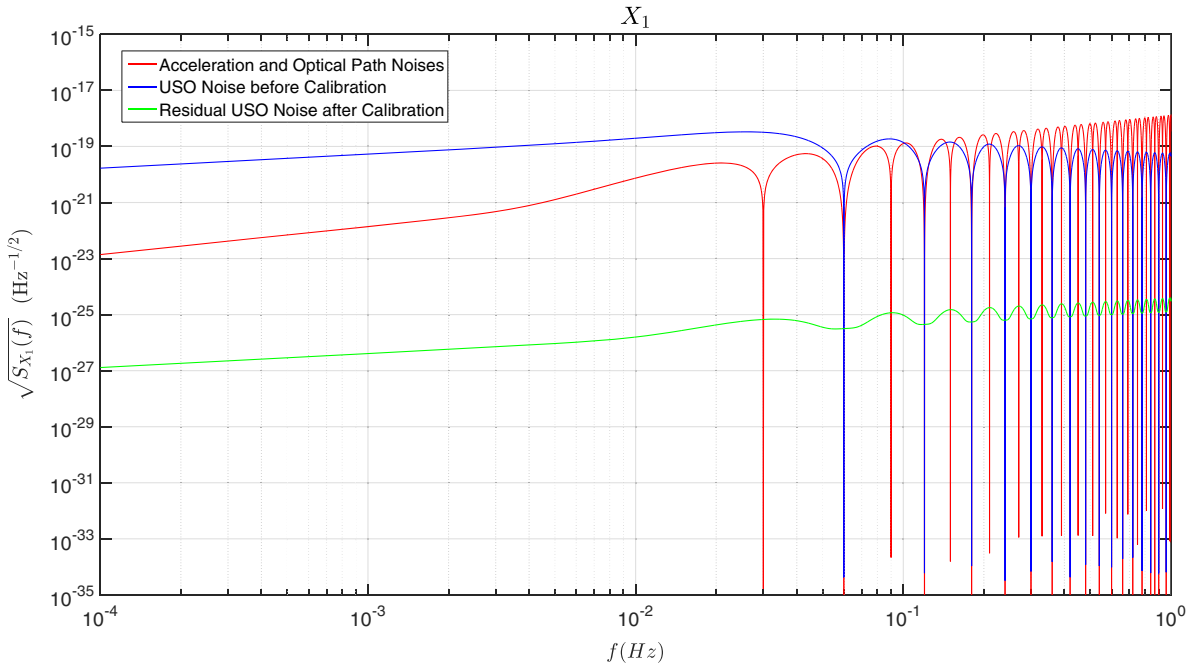

FIG. 3. Square root of the spectral densities of the fractional frequency fluctuations (strain) noises entering in the second-generation TDI combination X_1. The red line represents the contribution from the acceleration and optical-path noises. They jointly identify LISA's overall performance requirements. The blue line corresponds to the USO noise level in X_1 before the calibration procedure is applied, while the green line is the residual USO noise spectrum in X_1 after applying the calibration procedure. The beat-note magnitudes and signs have been chosen so as to result in the worst possible USO noise spectra (blue and green lines) in the X_1 TDI combination.

$$\alpha_1^{\mathrm{q}} = [\mathcal{D}_3\mathcal{D}_1\mathcal{D}_2 - I][(a_1 - a_{1'})q_1 + b_{1'}(I + \mathcal{D}_3\mathcal{D}_1\mathcal{D}_2)q_1 + [\mathcal{D}_{2'}\mathcal{D}_{1'}(b_{2'} - a_{2'}) + (a_2 - b_2)\mathcal{D}_3]q_2 + [\mathcal{D}_3\mathcal{D}_1(a_3 - b_3) + (b_{3'} - a_{3'})\mathcal{D}_{2'}]q_3], \tag{40}$$

after having factored out the delay operator $[\mathcal{D}_3\mathcal{D}_1\mathcal{D}_2 - I]$.

Since the expression inside the large square brackets is (apart from the primed delays due to the Sagnac effect) the same as that of the TDI-1 combination α given in Ref. [7], and because it was shown there that it is impossible to exactly calibrate out of α the USO noise using the r combinations [9], it follows that also for α_1^{q} it is impossible to exactly calibrate out the USO noise. As shown in Ref. [7], however, we can rewrite the USO phase noises in terms of some of the r data and only the USO phase noise q_1 by using the following additional identities:

$$\mathcal{D}_3\mathcal{D}_1\mathcal{D}_2 q_1 = q_1 - f_1[\mathcal{D}_3\mathcal{D}_1 r_3 + \mathcal{D}_3 r_2 + r_1], \tag{41}$$

$$\mathcal{D}_{2'}\mathcal{D}_{1'} q_2 = \frac{f_2}{f_1} q_1 - f_2[r_{1'} + \mathcal{D}_{2'} r_{3'}], \tag{42}$$

$$\mathcal{D}_3\mathcal{D}_1 q_3 = \frac{f_3}{f_1} q_1 - f_3[r_1 + \mathcal{D}_3 r_2], \tag{43}$$

$$\mathcal{D}_3 q_2 = \frac{f_2}{f_1} q_1 - f_2 r_1, \tag{44}$$

$$\mathcal{D}_{2'} q_3 = \frac{f_3}{f_1} q_1 - f_3 r_{1'}. \tag{45}$$

The USO noise terms involving the q_i in Eq. (40) then become

$$[(a_1 - a_{1'} + 2b_{1'})f_1 + (a_2 - a_{2'} + 2b_{2'})f_2 + (a_3 - a_{3'} + 2b_{3'})f_3]\frac{q_1}{f_1} - f_1 b_{1'}[r_1 + \mathcal{D}_3 r_2 + \mathcal{D}_3\mathcal{D}_1 r_3] - f_2[b_{2'} + a_2]r_1 - f_3[b_{3'} - a_{3'}]r_{1'} - f_2[b_{2'} - a_{2'}][r_{1'} + \mathcal{D}_{2'} r_{3'}] - f_3[b_{3'} + a_3][r_1 + \mathcal{D}_3 r_2]. \tag{46}$$

If we now take into account the expressions for the a and b coefficients, the first term in Eq. (46) can be reduced to the following form:

$$[(\nu_2-\nu_{3'})\dot{L}_1+(\nu_3-\nu_{1'})\dot{L}_2+(\nu_1-\nu_{2'})\dot{L}_3]\frac{q_1}{f_1}. \tag{47}$$

This corresponds to relative frequency fluctuations (or strain noise) of the order of about 10^{-27} under the assumptions of having laser frequency offsets of a few hundred megahertz, a laser center frequency equal to 3×10^{14} Hz, a Doppler term $\dot{L}_i$ equal to about 3×10^{-8}, and a USO frequency stability of about 10^{-13}. Thus, we can ignore it and, after some algebra, define the laser noise–free and USO noise–free reduced data α_1 to be

$$\begin{aligned}\alpha_1 \equiv \alpha_1^{\mathrm{q}} + [\mathcal{D}_3\mathcal{D}_1\mathcal{D}_2 - I]\Big[&\frac{1}{2}f_1 b_{1'}[(r_1+\mathcal{D}_3 r_2+\mathcal{D}_3\mathcal{D}_1 r_3)+(r_{1'}+\mathcal{D}_{2'}r_{3'}+\mathcal{D}_{2'}\mathcal{D}_{1'}r_{2'})]\\ &+f_2(b_{2'}+a_2)r_1+f_3(b_{3'}-a_{3'})r_{1'}+f_2(b_{2'}-a_{2'})(r_{1'}+\mathcal{D}_{2'}r_{3'})\\ &+f_3(b_{3'}+a_3)(r_1+\mathcal{D}_3 r_2)\Big].\end{aligned} \tag{48}$$

Like X_1, also α_1 should be antisymmetric with respect to permutation of the indices (2,3'), (3,2'), and (1,1'). The combinations in Eq. (46) used for calibrating out the USO noise from α_1^{q} have therefore, in Eq. (48), been antisymmetrized. The remaining two TDI-2 Sagnac responses, denoted α_2 and α_3, follow from Eq. (48) after performing cyclic permutation of the spacecraft indices.

In Fig. 4, we plot the square root of the power spectral densities of the relative frequency fluctuations (strain) associated with the noise sources entering the α_1 combination. These are the acceleration and optical-path noises (red line), the USO noise before it is calibrated out of α_1 (blue line), and the residual USO noise after applying the calibration procedure described in this subsection (green line). Like we did for the X_1 combination, here, too, we selected beat-note magnitudes and signs so as to result in the worst possible USO noise spectra (blue and green lines) in α_1. At 10^{-4} Hz, the residual USO noise is more than

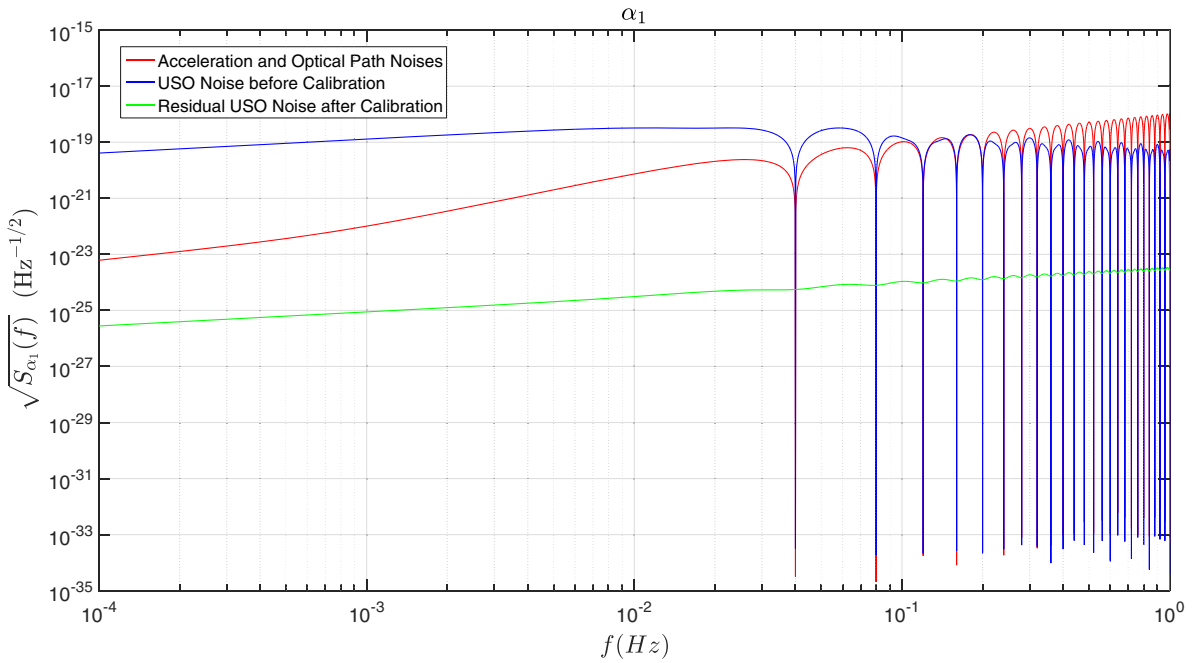

FIG. 4. Square root of the spectral densities of the fractional frequency fluctuations (strain) noises entering in the second-generation TDI combination α_1. The red line represents the contribution from the acceleration and optical-path noises. They jointly identify LISA's overall performance requirement. The blue line corresponds to the USO noise level in α_1 before the calibration procedure is applied, while the green line is the residual USO noise spectrum in α_1 after applying the calibration procedure. The beat-note magnitudes and signs have been chosen so as to result in the worst possible USO noise spectra (blue and green lines) in the α_1 TDI combination.

2 orders of magnitude smaller than the acceleration and optical-path noises, and it gets smaller at higher frequencies.

IV. CONCLUSIONS

This article addresses the problem of calibrating the onboard clock phase fluctuations out of the second-generation TDI combinations. We have focused our analysis on deriving calibrating expressions for the unequal-arm Michelson combination X_1 and the Sagnac combination α_1 as similar procedures can be extended to all other second-generation TDI combinations. Our approach relies on the key observation that the commutator of two delay operators applied to a LISA USO noise results in relative frequency fluctuations that are significantly smaller than those of the secondary noises and can therefore be neglected.

Although the sideband-sideband technique suppresses the LISA's USO noises to levels significantly smaller than that identified by the secondary noises, it does not cancel them exactly. This might result in a sensitivity limitation for more ambitious missions characterized by higher sensitivities and/or significantly larger beat notes [21,22]. This is because the calibrating algorithm presented here might not sufficiently suppress the USO noises in their TDI-2 combinations. The use of optical frequency comb, on the other hand, provides a solution in these cases by generating the microwave signal frequency coherent to the frequency of the onboard laser. This is because the optical frequency-comb technique exactly cancels the microwave signal phase fluctuations by using modified TDI-2 combinations and it does not require modulated beams.

In addition, use of an optical frequency comb may result in a simplification of LISA's onboard interferometry system [13] because (i) generation of modulated beams and additional heterodyne base-band measurements involving clock microwave sidebands will no longer be needed and (ii) the entire onboard USO subsystem can be replaced with the microwave signal referenced to the onboard laser. This may result in a reduced system complexity and the probability of subsystem failure. Recent progress in the realization of a space-qualified optical frequency comb indicates that such a capability will be available well before LISA's launching date [12].

ACKNOWLEDGMENTS

M. T. thanks Dr. Frank B. Estabrook and Dr. John W. Armstrong for their constant encouragement during the development of this work. O. H. gratefully acknowledges support from the Deutsches Zentrum für Luft- und Raumfahrt with funding from the Bundesministerium für Wirtschaft und Technologie (Project No. 50OQ1601). Finally, we thank an anonymous referee for many valuable and helpful comments.

[1] B. P. Abbott *et al.* (LIGO Scientific and Virgo Collaborations), Phys. Rev. Lett. **116**, 061102 (2016).
[2] B. P. Abbott *et al.* (LIGO Scientific and Virgo Collaborations), Phys. Rev. Lett. **116**, 241103 (2016).
[3] B. P. Abbott *et al.* (LIGO Scientific and Virgo Collaborations), Phys. Rev. Lett. **118**, 221101 (2017).
[4] B. P. Abbott *et al.* (LIGO Scientific and Virgo Collaborations), Phys. Rev. Lett. **119**, 141101 (2017).
[5] B. P. Abbott *et al.* (LIGO Scientific and Virgo Collaborations), Phys. Rev. Lett. **119**, 161101 (2017).
[6] P. Amaro-Seoane *et al.*, arXiv:1702.00786.
[7] M. Tinto, F. B. Estabrook, and J. W. Armstrong, Phys. Rev. D **65**, 082003 (2002).
[8] R. Hellings, G. Giampieri, L. Maleki, M. Tinto, K. Danzmann, J. Hough, and D. Robertson, Opt. Commun. **124**, 313 (1996).
[9] R. W. Hellings, Phys. Rev. D **64**, 022002 (2001).
[10] J. L. Hall, Rev. Mod. Phys. **78**, 1279 (2006).
[11] T. W. Hänsch, Rev. Mod. Phys. **78**, 1297 (2006).
[12] M. Giunta *et al.*, in *Conference on Lasers and Electro-Optics* (Optical Society of America, Washington, DC, 2016), p. STh4H.5.
[13] M. Tinto and N. Yu, Phys. Rev. D **92**, 042002 (2015).
[14] M. Otto, *Time-delay Interferometry Simulations for the Laser Interferometer Space Antenna* (Technische Informationsbibliothek, Hannover, 2015).
[15] M. Otto, G. Heinzel, and K. Danzmann, Classical Quantum Gravity **29**, 205003 (2012).
[16] M. Tinto and S. V. Dhurandhar, Living Rev. Relativity **17**, 6 (2014).
[17] V. Leonhardt and J. B. Camp, Appl. Opt. **45**, 4142 (2006).
[18] W. Kokuyama, K. Numata, and J. Camp, Appl. Opt. **49**, 6264 (2010).
[19] S. Barke, Ph. D. thesis, Hanover University, 2015, http://simonbarke.com/download/Simon_Barke-PhD_Thesis_2015-vorgelegt.pdf.
[20] J. A. Barnes *et al.*, IEEE Trans. Instrum. Meas. **IM-20**, 105 (1971).
[21] J. Crowder and N. J. Cornish, Phys. Rev. D **72**, 083005 (2005).
[22] W. Gang and N. Wei-Tou, Chin. Phys. B **22**, 049501 (2013).